Acoustic modification of collagen hydrogels facilitates cellular remodeling

E.G. Norris [a], D. Dalecki [b], D.C. Hocking [a,b,*]

[a] Department of Pharmacology and Physiology, University of Rochester School of Medicine and Dentistry, Rochester, NY 14642, USA
[b] Department of Biomedical Engineering, University of Rochester, Rochester, NY 14627, USA

A B S T R A C T

Developing tunable biomaterials that have the capacity to recreate the physical and biochemical characteristics of native extracellular matrices (ECMs) with spatial fidelity is important for a variety of biomedical, biological, and clinical applications. Several factors have made the ECM protein, collagen I, an attractive biomaterial, including its ease of isolation, low antigenicity and toxicity, and biodegradability. However, current collagen gel formulations fail to recapitulate the range of collagen structures observed in native tissues, presenting a significant challenge in achieving the full potential of collagen-based biomaterials. Collagen fiber structure can be manipulated in vitro through mechanical forces, environmental factors, or thermal mechanisms. Here, we describe a new ultrasound-based fabrication technology that exploits the ability of ultrasound to generate localized mechanical forces to control the collagen fiber microstructure non-invasively. The results indicate that exposing soluble collagen to ultrasound (7.8 or 8.8 MHz; 3.2–10 W/cm^2) during hydrogel formation leads to local variations in collagen fiber structure and organization that support increased levels of cell migration. Furthermore, multiphoton imaging revealed increased cell-mediated collagen remodeling of ultrasound-exposed but not sham-exposed hydrogels, including formation of multicellular aggregates, collagen fiber bundle contraction, and increased binding of collagen hybridizing peptides. Skin explant cultures obtained from diabetic mice showed similar enhancement of cell-mediated remodeling of ultrasound-exposed but not sham-exposed collagen hydrogels. Using the mechanical forces associated with ultrasound to induce local changes in collagen fibril structure and organization to functionalize native biomaterials is a promising non-invasive and non-toxic technology for tissue engineering and regenerative medicine.

1. Introduction

Collagen-based hydrogels are used extensively for clinical, pharmaceutical, and research applications. Type I collagen is the primary structural component of native extracellular matrices (ECMs) and the most abundant protein found in vertebrates [1]. Accordingly, large quantities of collagen can be purified from tissues via enzymatic or acid digestion and then reconstituted into pure or composite hydrogels for various purposes [2,3]. Currently, collagen I is used in wound dressings and for skin substitutes; it is also a common component of biomaterials used in biological research and investigated for tissue-engineering purposes [2–4]. Collagen gel systems are being developed for a variety of bioengineering platforms, including tissue scaffolds, in vitro cell culture models, and stem cell and drug-delivery vehicles [5,6]. Several factors make collagen I an attractive biomaterial, including its ease of isolation,

low antigenicity and toxicity, and biodegradability [3]. However, current collagen gel formulations fail to recapitulate the range of collagen structures observed in native tissues, presenting a significant challenge in achieving the full potential of collagen-based biomaterials [4,7]. Thus, considerable effort has been directed at developing methods to improve on the inherent biocompatibility and bioactive properties of collagen to produce materials for regenerative medicine applications [2].

Collagen I is the principal component of bone, tendons, skin, ligaments, and cornea and is found in most interstitial connective tissues, where it provides tensile strength to tissues, regulates cell adhesion, and facilitates cell migration [1]. The incredible diversity of functional properties of collagen I arises from variations in the micromolecular and macromolecular structure of polymerized collagen fibers [8]. Collagen hydrogels are easily formed in vitro by increasing the temperature of a neutralized ice-cold solution of soluble collagen to between 20 and 37 °C

[9]. The physical properties of self-assembled collagen fibers, including fibril density, thickness, and alignment, are influenced by several factors, including collagen concentration, temperature, pH, ionic strength, and applied mechanical forces [2]. Several groups have exploited these critical collagen self-assembly parameters to vary the density and diameter of collagen fibers and produce collagen-based biomaterials with desired structural features [10–14]. Non-toxic and non-invasive fabrication technologies that harness these parameters to recreate various collagen fiber structures rapidly would provide a next-generation approach to regulate the biological properties of collagen-based biomaterials and thereby control cellular responses during tissue regeneration. Moreover, advanced biomaterials with regionally defined variations in collagen fiber structure and function could provide spatial cues to instruct cell behavior and drive three-dimensional (3D) tissue formation.

Ultrasound (US) is a versatile tool for influencing biological systems for therapeutic benefit. US-based technologies offer several key advantages in clinical translation, including a long history of safety and the ability to be applied non-invasively with high spatial precision [15]. US fields can interact with biomaterials and tissues through either thermal or non-thermal, mechanical mechanisms [16,17]. Absorption of US by tissue components, including collagen, results in the conversion of ultrasonic energy to heat [18,19]. In addition, US can exert localized compression, tensile, and shear forces via mechanical mechanisms, such as radiation force, acoustic streaming, and cavitation [16,17]. Importantly, many of the known biological effects of US, including heating and fluid streaming, have the potential to influence collagen structure [10,16,20]. Our previous studies demonstrated that US fields could be designed to non-invasively control collagen fiber length and diameter in a site-specific manner within 3D hydrogels [21]. In the present study, we identify US exposure parameters that produce collagen hydrogels with enhanced cell migration and matrix remodeling capacity and characterize the structural properties of acoustically modified hydrogels. Together, the results demonstrate that US can be used to create complex, 3D collagen architectures that support coordinated cell responses essential for tissue remodeling.

2. Methods

2.1. Generation and characterization of acoustic fields

US fields were generated using a single-element, piezoceramic transducer. The US transducer was mounted to the bottom of a plastic exposure tank filled with degassed, deionized water (Fig. 1). Two different acoustic sources were used for experiments. One transducer had a diameter of 0.6 cm and a fundamental frequency of 7.8 MHz; the other transducer had a diameter of 1.0 cm and a fundamental frequency of 8.8 MHz. The water temperature in the exposure tank was controlled using a circulating water heater (VWR, 1122). The acoustic source was driven by a continuous, sinusoidal signal produced by a function generator (Tektronix, AFG3022B). The amplitude of the signal was adjusted using an attenuator (Kay 837) and a radio frequency power amplifier (ENI, 2100 L). Acoustic pressure amplitude as a function of spatial location (i.e., beam pattern) was measured using both needle (Onda, HNC-0400) and capsule (Onda, HGL-0085) hydrophones. The half-maximal transaxial beam width was 3 mm at a position of 4.9 cm from the 7.8-MHz transducer and 10.5 cm from the 8.8-MHz transducer. These axial positions were chosen as the exposure locations for collagen samples.

Acoustic pressures and intensities (spatial peak, pulse average intensity, I_{sppa}) at the exposure location were calibrated before and after each experiment. Transducer properties and exposure parameters are detailed in Table 1. Non-linear acoustic propagation effects were evidenced by the asymmetry of peak positive and peak negative pressures for each exposure condition investigated [22,23]. Exposure conditions were selected such that similar levels of US-induced heating were produced with the two transducers. Measurements of I_{sppa} and maximum temperature within collagen samples for all exposure conditions are summarized in Table 1.

2.2. Collagen gel preparation and US exposure

Native type I collagen gels were prepared as described previously [21]. In brief, degassed solutions of 2X concentrated Dulbecco's modified Eagle medium (DMEM, Gibco) and 1 X DMEM with 4-(2-hydroxyethyl)-1-piperazineethanesulfonic acid (HEPES) were combined with type I rat tail collagen (in 20 mM acetic acid; Corning) such that the final concentrations were 0.8 mg/mL collagen in 1X DMEM with 15 mM HEPES. In some experiments, the final collagen concentration was 2 mg/mL. Oregon green-labeled collagen was prepared by conjugating 1 mg/mL type I rat tail collagen with Oregon Green 488 (Molecular Probes), as described previously [24]. All reagents were prechilled to 4 °C, and neutralized collagen solutions were maintained on ice before acoustic exposures. To initiate collagen gel formation, aliquots of neutralized collagen were pipetted into one well of an elastomer-bottomed tissue culture plate (6-well; 2.5- or 3.7-cm diameter; FlexCell Corp) [21]. The plates were positioned at the water surface using a three-axis positioner (Series B4000, Unislide; Velmex) such that the center of the well was at the calibration location. Collagen solutions were exposed to a continuous wave US field at a center frequency of either 7.8 or 8.8 MHz, with acoustic intensities ranging from 3.2 to 10 W/cm². Samples were exposed to US for 15 min, with a water tank temperature of 25 °C. These conditions were sufficient to allow for the spontaneous polymerization of soluble collagen monomers into hydrogels. Sham-exposed collagen gels were polymerized in the exposure tank for the same amount of time but were not exposed to US. For sham-exposed gels, the water temperature in the exposure chamber was varied between 25 and 37 °C to achieve temperatures within the collagen samples that matched those achieved during US exposures (Table 1). After either US or sham exposure, the samples were incubated for an additional 1 h at 37 °C and 8% CO_2 to complete collagen polymerization. An equal volume of cell culture media (1:1 mixture of Aim V [Gibco] and SF Medium [Corning]) was overlaid on gels, followed by an overnight incubation to allow for media equilibration. The thickness of collagen gels after polymerization was 5 mm.

2.3. Temperature measurements

Temperature as a function of time was measured in collagen samples during US and sham exposures using type-T wire thermocouples
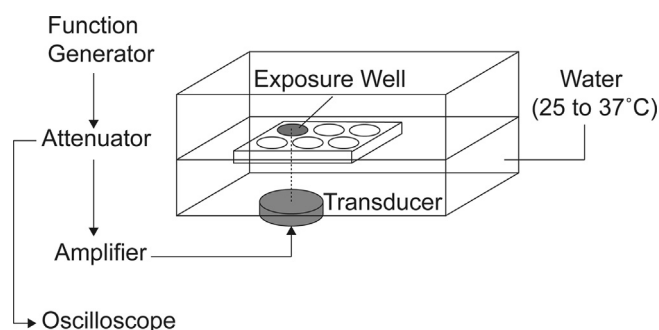

Fig. 1. Schematic of the ultrasound exposure system. Ultrasound fields were generated using an unfocused piezoceramic transducer with a center frequency of 7.8 or 8.8 MHz. Transducers were fixed to the bottom of a temperature-controlled exposure tank filled with degassed, deionized water. Acoustic fields were generated using a function generator, with the amplitude controlled using an attenuator and amplifier, and monitored throughout the exposure using a digital oscilloscope. Sample holders were positioned using a three-axis positioner such that the well bottoms were in contact with the water, and the center of the exposure well was located 4.9 cm (7.8 MHz) or 10.5 cm (8.8 MHz) away from the transducer face. At this location, the half-maximal beam width was 3 mm.

Table 1
Summary of acoustic exposure conditions.

Transducer 1: 0.6-cm diameter, 7.8-MHz center frequency, exposure site = 4.9 cm from the transducer				
Water tank temperature (°C)	Peak positive pressure	Peak negative pressure	Acoustic intensity (I_{sppa})	Peak Temperature
25 °C	0.34 ± 0.004 MPa	0.27 ± 0.005 MPa	3.2 ± 0.07 W/cm^2	27.9 ± 0.3 °C
25 °C	0.54 ± 0.003 MPa	0.37 ± 0.005 MPa	6.8 ± 0.09 W/cm^2	30.2 ± 0.2 °C
25 °C	0.70 ± 0.004 MPa	0.44 ± 0.006 MPa	10.4 ± 0.1 W/cm^2	32.2 ± 0.5 °C
Transducer 2: 1-cm diameter, 8.8-MHz center frequency, exposure site = 10.5 cm from the transducer				
Water tank temperature (°C)	Peak positive pressure	Peak negative pressure	Acoustic intensity (I_{sppa})	Peak temperature
25 °C	0.47 ± 0.02 MPa	0.29 ± 0.02 MPa	3.8 ± 0.09 W/cm^2	27.7 ± 0.1 °C
25 °C	0.74 ± 0.02 MPa	0.44 ± 0.02 MPa	8.0 ± 0.09 W/cm^2	33.0 ± 0.2 °C
Sham exposure conditions				
Water tank temperature (°C)	Peak positive pressure	Peak negative pressure	Acoustic intensity (I_{sppa})	Peak temperature
25 °C	0 MPa	0 MPa	0 W/cm^2	24.5 ± 0.01 °C
30 °C	0 MPa	0 MPa	0 W/cm^2	28.4 ± 0.3 °C
33 °C	0 MPa	0 MPa	0 W/cm^2	30.5 ± 0.04 °C
37 °C	0 MPa	0 MPa	0 W/cm^2	34.5 ± 0.1 °C

I_{sppa}, spatial peak, pulse average intensity; SEM, standard error of the mean.
Ultrasound fields were generated using an unfocused piezoceramic transducer with diameter and center frequency as indicated. Fields were calibrated using a capsule hydrophone at a position in the free field such that the half-maximum beam width was 3 mm. Field parameters are reported for each exposure condition. The temperature within a polymerizing collagen sample was measured using a wire thermocouple embedded at the center of the gel. The peak temperature achieved in each sample was averaged over the final minute of ultrasound exposure, by which point the temperature had stabilized. The difference in the final temperature was not statistically significant for 0.8 mg/mL and 2.0 mg/mL collagen samples. Data are presented as the mean ± SEM. n ≥ 9 for pressure and intensity measurements; n ≥ 3 for temperature measurements.

(Physitemp), as described previously [21]. In brief, thermocouples were placed within the elastomer-bottomed tissue culture wells such that the thermocouple junction was at the center of the well and 2.5 mm above the bottom of the well. A three-axis positioner was used to precisely position the plate such that the thermocouple junction was located at the center of the US beam. The cold, neutralized collagen solution was then added to the well and exposed to US. The temperature at the thermocouple junction was recorded at 15-s intervals for 15 min using a digital thermometer (BAT-12, Physitemp).

2.4. Cell migration assay

Fibronectin-null mouse embryonic fibroblasts (FN-null MEFs) were cultured in a 1:1 mixture of Aim V and SF Medium, as described previously [25]. The FN-null MEFs were seeded at a density of 4.7×10^4 cells/cm^2 onto collagen gels prepolymerized under either US or sham exposure conditions. Cell-seeded collagen gels were incubated at 37 °C and 8% CO$_2$ for up to 24 h. The distribution of cells on the collagen gel surface was visualized at 20 min and 24 h after seeding using an BX-60 upright microscope (Olympus), and phase-contrast images were obtained using a digital camera (QImaging). To visualize an area encompassing the half-maximal beam width of the US field, overlapping images of the central surface of each gel were collected and assembled into 3.5 mm × 3.5 mm panoramic images using Photoshop software (Adobe). At each time point, regions of the collagen gel surface that did not contain cells were outlined and measured using FIJI software (NIH). The difference in the cell-free area between the 24-h and the initial 20-min time points was used to quantify the extent of cell migration. In some experiments, cell-seeded collagen gels were fixed with 2% paraformaldehyde in phosphate-buffered saline (PBS) for subsequent multiphoton imaging.

2.5. Cell adhesion assay

FN-null MEFs were seeded at a density of 2×10^4 cells/cm^2 onto collagen gels (2 mg/mL) polymerized under either US or sham exposure conditions. In some experiments, cells were preincubated with 25 μg/mL of the following antibodies before seeding: anti-β1 integrin (clone Ha2/5), anti-β3 integrin (clone 2C9.G2), or IgG and IgM isotype controls (BD

Biosciences). Cell-seeded collagen gels were incubated for 20 min at 37 °C and 8% CO$_2$ and then washed with PBS to remove non-adherent cells. Collagen gel surfaces were subsequently imaged using phase-contrast microscopy. Two regions of interest (2.2 mm × 1.7 mm) were selected from each gel, one located at the center of the US-exposed area and one located outside the beam area (4 mm off-center). The number of adherent cells within each region of interest was quantified using FIJI software (NIH).

2.6. Collagen remodeling assay

FN-null MEFs were seeded at a density of 4.7×10^4 cells/cm^2 onto collagen gels polymerized under US or sham exposure conditions. A corresponding set of US- or sham-exposed collagen gels received an equal volume of media alone ('acellular'). Collagen gels were incubated at 37 °C and 8% CO$_2$ for 24 h. The media was removed, and the gels were treated with Triton X-100 extraction buffer (25 mM Tris-HCl, pH 9.6,1% Triton X-100, 10 mM ethylene glycol-bis(β-aminoethyl ether)-N,N,N′,N′-tetraacetic acid (EGTA), and protease inhibitor cocktail [SigmaFAST 8830, Sigma Aldrich]) for 5 min at RT to remove adherent cells [26]. Acellular collagen gels were treated similarly. Gels were washed extensively with PBS and incubated overnight at 4 °C with fluorescein-tagged collagen hybridizing peptides (CHPs; 3Helix), diluted in PBS to a final concentration of 4 μM. Unbound CHPs were removed, and the gels were washed with PBS and then fixed with 2% paraformaldehyde in PBS for 1 h at room temperature before multiphoton imaging.

2.7. Multiphoton microscopy

Collagen fibers were visualized by second harmonic generation (SHG) microscopy, using a Fluoview 1000 AOM-MPM or FVMPE-RS microscope equipped with a 10X (0.45 NA) or a 25X (NA 1.05) objective, respectively (Olympus). The samples were illuminated with an 800-nm light generated by a Mai Tai HP Deep See Ti:Sa laser. Emitted light was detected using a photomultiplier tube through band-pass filters of either 370–410 (collagen SHG) or 495–540 (cellular autofluorescence or fluorescein-CHP). Images images were collected at representative locations within the area of interest through a depth of 100 μm in 5-μm z-steps, beginning

at the collagen gel surface. Maximum-intensity axial projections were reconstructed using FIJI software (NIH). Each experimental condition included at least 3 gels fabricated on independent days; 3–5 representative images were collected from within the US-exposed region of each gel or from the corresponding center of sham-exposed gels. Panoramic images were assembled from overlapping images collected at the center of the gel over an area that corresponded to the 3-mm half-maximal beam width of the US field. Single slices from the same depth (acellular samples) or maximum-intensity z-projections (cell-seeded samples) were assembled using Photoshop (Adobe).

2.8. Skin explant culture

Genetically diabetic male mice (BKS.Cg-*Dock7^m* +/+ Lepr^db^/J; Jackson Laboratory No. 000642) were housed in accordance with protocols reviewed and approved by the University Committee on Animal Resources at the University of Rochester Medical Center. Full-thickness skin biopsy sections were collected from the dorsal side of individual animals using a 6-mm biopsy punch. The tissue biopsies were washed with cell culture media and placed dermis-side down on the surface of collagen gels polymerized under US- or sham-exposed conditions. Skin explants were cultured for 3 days at 37 °C and 8% CO_2 to allow for cell attachment and dispersion onto the collagen surface. Cell culture media (0.37 mL/cm^2) were then added to wells, and explants were removed. Phase-contrast images of the collagen gel surface were collected immediately after removing the tissue explant ('day 3'). Collagen-adherent cells were incubated for an additional 4 days at 37 °C and 8% CO_2, and phase-contrast images were again obtained ('day 7').

2.9. Statistical analyses

Cellular adhesion and migration data were analyzed for statistical significance using Prism software (version 8, GraphPad). One-way analyses of variance were followed by the Bonferroni correction for multiple comparisons for at least 3 gels fabricated on independent days per condition.

3. Results

3.1. Effects of US on collagen fiber organization

To investigate how US exposure affects the structure of collagen fibers, US- and sham-exposed collagen hydrogels were analyzed using SHG microscopy, and panoramic images were reconstructed to visualize regions spanning the entire half-maximal beam width (3 mm) of the acoustic field. As reported previously [21], sham-exposed collagen hydrogels polymerized at 25 °C were characterized by short, randomly oriented fibers that were homogeneously distributed through the gel (Fig. 2A). In contrast, collagen fibers of hydrogels polymerized in the presence of 7.8-MHz US exhibited distinct structural features and spatial arrangements that varied with US intensity. Collagen gels exposed to US at an intensity of 3.2 W/cm^2 exhibited radially aligned fibers that extended outward from the center of the exposure site (Fig. 2B). Similar radial fiber alignment, as well as regions with increased collagen fiber density, was observed within collagen hydrogels exposed to US at the higher intensity of 6.8 W/cm^2 (Fig. 2C). When exposed to the highest intensity tested (10 W/cm^2), collagen gels showed a broad range of fibrillar structures, with regions of increased
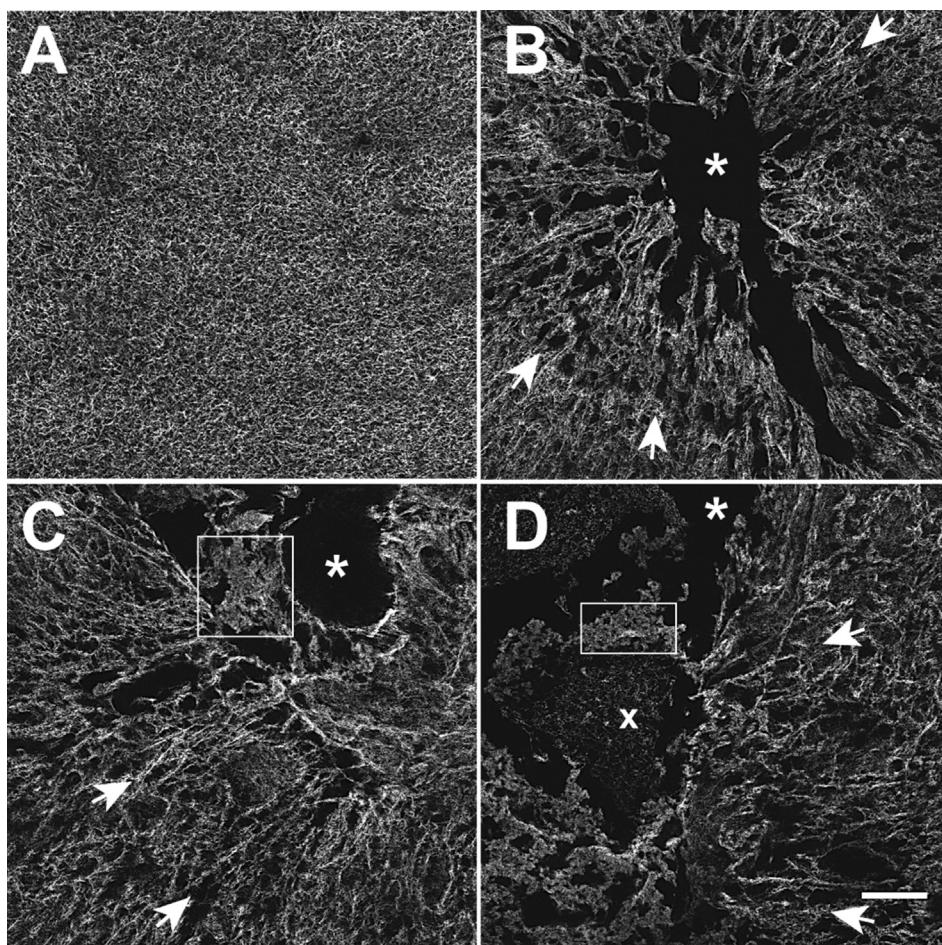

Fig. 2. Collagen fiber organization in ultrasound-exposed collagen hydrogels. Neutralized solutions of type I collagen were exposed to 7.8-MHz ultrasound at intensities of 0 (sham) (A), 3.2 (B), 6.8 (C), or 10 W/cm^2 (D) for 15 min. Collagen fibers were visualized after exposure using SHG microscopy. For each gel, multiple overlapping images were collected at an average depth of 250 μm beneath the hydrogel surface and reconstructed using Photoshop software, providing a field of view perpendicular to the sound field and encompassing the half-maximal beam width (3 mm). Representative images show features present in acoustically modified collagen gels, including radial fiber alignment (arrows), increased fiber density (boxes), short fibers (X), and absent/reduced collagen content (asterisks). Scale bar = 500 μm. SHG, second harmonic generation.

collagen fiber alignment and density interspersed with areas having an attenuated SHG signal (Fig. 2D). In contrast to sham-exposed gels, US-exposed samples also exhibited regions without a detectable SHG signal (Fig. 2, asterisks). Similar patterns were observed in US-exposed collagen hydrogels in which Oregon Green[488]–conjugated collagen was included as a tracer molecule (Fig. S1), indicating that collagen in these regions was markedly reduced or absent. Taken together, these results indicate that exposing collagen to US during hydrogel formation leads to specific changes in collagen fiber structure and organization, including radial fiber alignment and increased collagen fiber density, and introduces regions of interconnected porosity. Furthermore, these structural variations are present within the same gel at spatially distinct locations.

3.2. Non-thermal effects of US on collagen structure

US exposures at frequencies and intensities similar to those used in the present study can cause heating within tissue culture systems, and this temperature rise may influence collagen structure [10,21,27]. Therefore, studies were conducted to evaluate the contribution of US-induced heating to the changes in collagen structure observed in response to 7.8-MHz US over the range of acoustic intensities used (3.2, 6.8, and 10 W/cm^2). For initial studies, the water temperature in the exposure chamber was maintained at 25 °C. In the absence of US, the temperature within the collagen samples increased over 15 min from 4 °C to 24.5 ± 0.01 °C (Fig. 3A, sham). In the presence of US, heating during collagen polymerization progressed in two stages, wherein the temperature first stabilized close to water temperature after 4–5 min of exposure, and then underwent a second heating phase approximately 6 min into the exposure (Fig. 3A; 3.2, 6.8, and 10 W/cm^2). As expected [28], the maximum temperature reached at the center of each gel increased with acoustic intensity, with a maximum temperature of 32.2 ± 0.5 °C recorded in the 10 W/cm^2 condition (Fig. 3A). Subsequent experiments were conducted to identify water tank temperature conditions that produced heating profiles in sham-exposed collagen gels similar to those produced by US. To do so, the water temperature in the exposure chamber was increased to 30, 33, or 37 °C, and temperatures at the center of collagen samples polymerized under sham-exposure conditions were recorded over 15 min (Fig. 3B). The maximum temperature achieved at the gel center, under each set of polymerization conditions, is summarized in Table 1.

To determine whether US-induced heating was sufficient to produce the observed changes in the collagen microstructure, the structure and organization of collagen fibers of hydrogels exposed to 7.8-MHz US at intensities of 3.2, 6.8, or 10 W/cm^2 were compared with temperature-matched, sham-exposed collagen gels. Consistent with the results shown in Fig. 2, US-exposed collagen exhibited regions of radially aligned collagen fiber bundles, with heterogeneous regions of variable SHG intensity (Fig. 3C, top row). In contrast, the corresponding temperature-matched collagen gels polymerized under sham exposure conditions were characterized by randomly oriented, similar-sized fibrillar structures (Fig. 3C, bottom row). These results demonstrate that heating alone is not sufficient to replicate the effects of US on collagen fiber structure and organization.

3.3. Acoustically modified collagen supports directional cell migration

Collagen fiber structure and organization are key determinants of cell behaviors within both engineered biological constructs and physiological systems [10,11,29]. Therefore, we next investigated whether US exposure during polymerization affects the capacity of collagen to support cell migration. FN-null MEFs were used for these studies as these cells do not produce fibronectin endogenously and are cultured in a defined medium that lacks fibronectin and other adhesive proteins [30]. These culture conditions limit cell-mediated ECM deposition and thereby direct cells to use the acoustically modified substrate for adhesion and migration [30, 31]. Of note, cells were not exposed directly to US. Rather, collagen gels were fabricated under US or sham exposure conditions, and the cells were subsequently seeded onto the surface of fully polymerized collagen hydrogels.
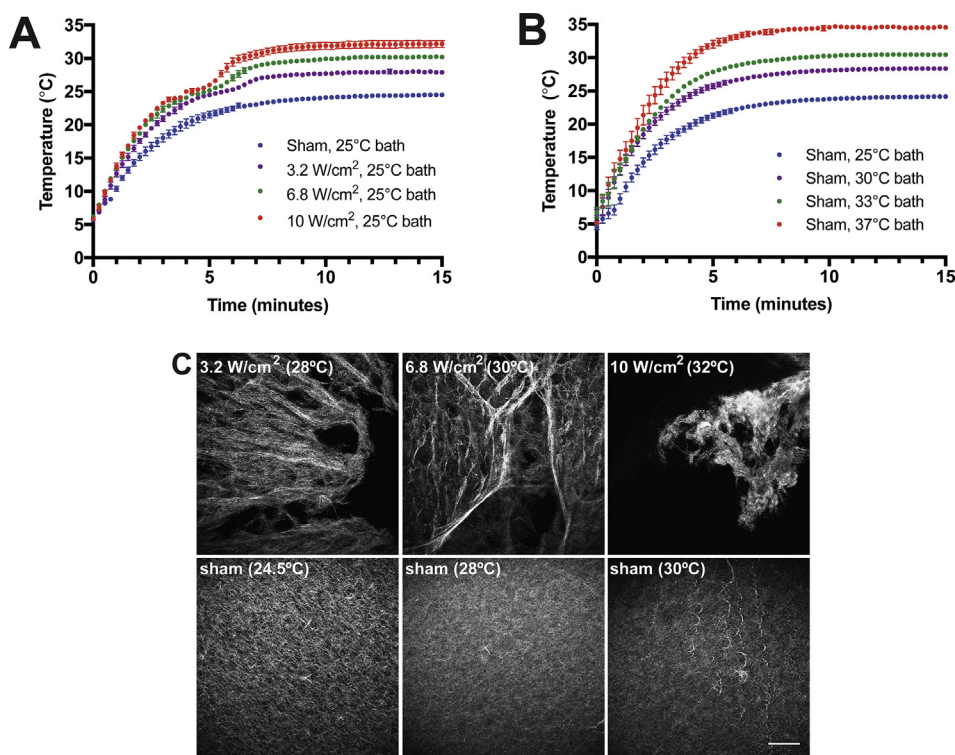

Fig. 3. Non-thermal effects of ultrasound on collagen structure (A) The temperature of collagen solutions was measured at the center of the acoustic beam during exposure to 7.8-MHz ultrasound at intensities of 0 (sham), 3.2, 6.8, or 10 W/cm^2. Exposures were conducted with the water temperature of the exposure chamber set to 25 °C. (B) The water temperature in the exposure tank was adjusted (to 25, 30, 33, or 37 °C) such that the maximum temperatures reached in sham-exposed collagen gels were comparable with those observed in ultrasound-exposed samples. Data are presented as the mean temperature ± SEM for n ≥ 3 replicates per condition. (C) Neutralized collagen solutions were polymerized for 15 min in a 25 °C water bath while being exposed to 7.8-MHz ultrasound with the indicated acoustic intensities (top row) or under sham exposure conditions with water temperatures adjusted to 25, 30, or 33 °C to achieve maximum temperatures of 24.5, 28, or 30 °C, respectively (bottom row). The maximum temperature achieved in each condition is reported in parentheses. Polymerized gels were imaged using SHG microscopy. Maximum intensity projections were assembled from Z-slices (5-μm step size) collected beginning at the collagen surface and extending 100 μm into the gel. Images represent 1 of at least 3 experiments from gels fabricated on independent days. Scale bar = 200 μm. SEM, standard error of the mean; SHG, second harmonic generation.

To assess effects of acoustic modification on the ability of collagen hydrogels to support cell migration, the distribution of cells on the surface of collagen hydrogels, fabricated in the absence and presence of 7.8-MHz US at intensities of 3.2, 6.8 or 10 W/cm^2, was examined at 20 min and 24 h after seeding. Twenty minutes after seeding, the cells were distributed evenly across the surfaces of gels fabricated using US intensities of 3.2 or 6.8 W/cm^2 (Fig. 4A, 20 min). Cells seeded onto collagen gels exposed to US at an intensity of 10 W/cm^2 adhered to much of the surface but did not adhere to regions corresponding to the very center of the acoustic field (Fig. 4A, 20 min), consistent with the reduced collagen content found at this location (Fig. 2D). After 24 h of culture, large areas of cellular reorganization were observed on US-exposed (Fig. 4A) but not sham-exposed

(Fig. S2) gels. Specifically, on gels exposed to US at intensities of 3.2 and 6.8 W/cm^2, cells collectively migrated into radially aligned linear clusters, leaving behind large cell-free areas on the gel surface (Fig. 4A, 24 h). Similarly, large cell aggregates were observed on the surface of collagen hydrogels polymerized in the presence of 7.8-MHz US at 10 W/cm^2, with an expansion of the initial cell-free areas (Fig. 4A, 24 h). In contrast, cells were homogeneously distributed on temperature-matched, sham-exposed collagen gels, and no change in overall cell distribution was observed over 24 h (Fig. S2). Global cell migration was subsequently quantified as the difference in cell-free areas between the 24-h and 20-min time points. The largest effect on cell migration was observed with collagen gels exposed to US at an intensity of 6.8 W/cm^2 (Fig. 4B).
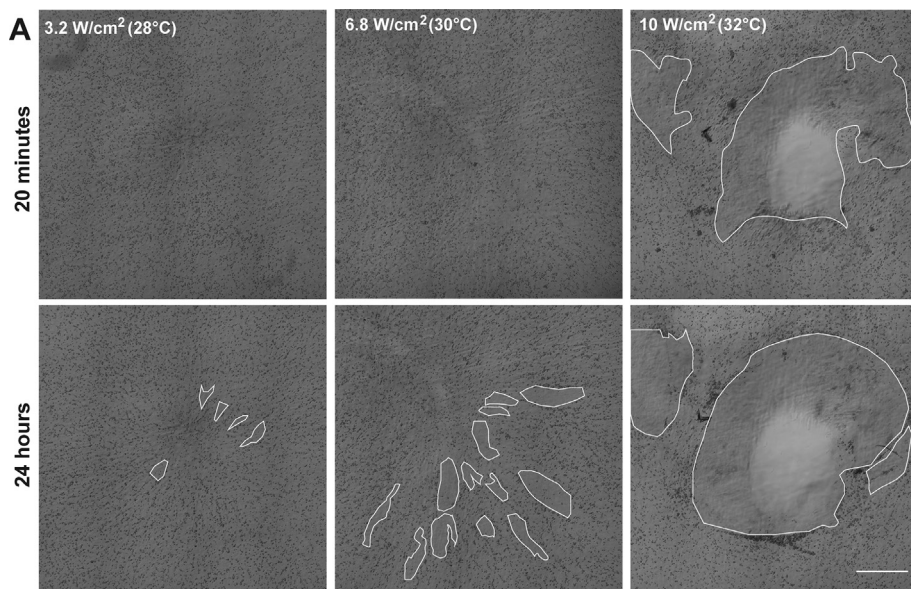

Fig. 4. Cell migration on acoustically modified collagen hydrogels. Aliquots of soluble collagen were exposed to 7.8-MHz ultrasound at the indicated acoustic intensities. The maximum temperature achieved under each set of acoustic exposure conditions is indicated in parentheses. FN-null MEFs (4.7 × 10^4 cells/cm^2) were seeded onto the surface of polymerized gels. Phase-contrast images were collected at 20 min and 24 h after seeding. Overlapping images captured within the ultrasound-exposed area were merged to reconstruct an image area representing the entire half-maximal ultrasound beam width (3 mm). (A) Representative images are shown from 1 of at least 4 independent experiments. Cell-free areas in each image were traced using FIJI software (white outlines). Scale bars = 1 mm. (B) The total area of cell migration was determined as the difference in cell-free areas between 24 h and 20 min for each condition. Data are presented as the mean ± SEM for n ≥ 4. *P<0.05 by one-way ANOVA with Bonferroni's post-hoc test. FN-null MEFs, fibronectin-null mouse embryonic fibroblasts; SEM, standard error of the mean.
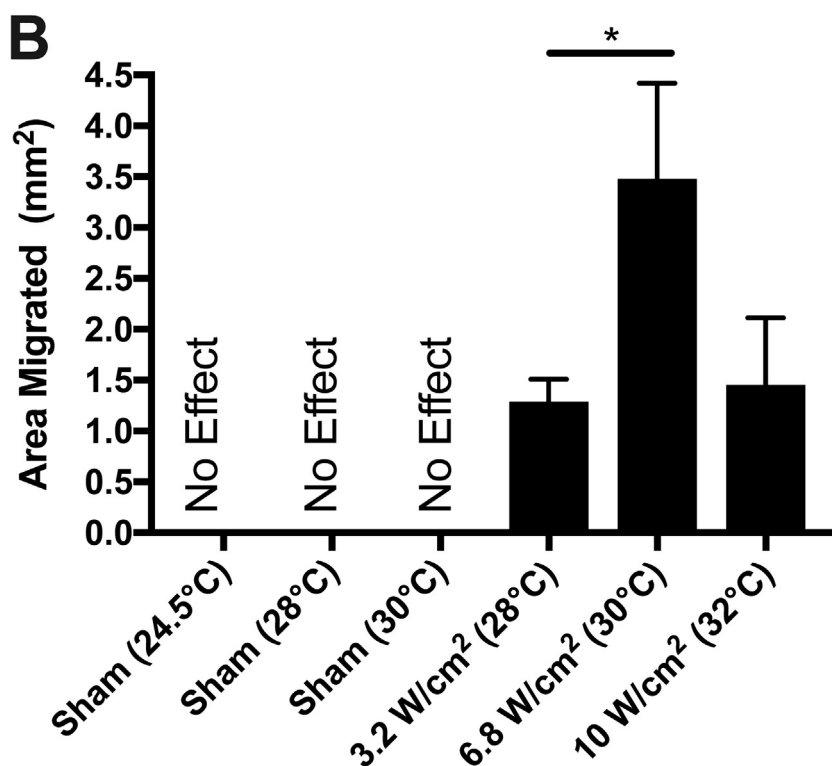
3.4. Acoustic modification reduces β1 integrin–mediated cell adhesion

The strength of integrin-mediated cell-substrate contacts influences both cell attachment and migration [32]. Thus, cell adhesion assays were used to determine how exposing collagen to US affects subsequent cell attachment to polymerized gels. For these studies, the collagen concentration was increased to 2.0 mg/mL, which eliminated the central pore introduced by US exposure and allowed for the homogenous distribution of cells on the gel surface. The number of cells adherent 20 min after seeding was used as an indicator of initial adhesion strength [33]. Compared with sham-exposed controls, cell attachment to the US-exposed region was significantly reduced on collagen gels polymerized during exposure to 8.8-MHz US at an intensity of 8 W/cm^2 (Fig. 5A). The reduction in adhesion observed in US-exposed samples was not replicated by temperature-matched, sham-exposed gels (Fig. 5A), indicating that the effects of US exposure on cell adhesion to collagen were not mediated by US-induced heating. Importantly, similar numbers of cells adhered to sham-exposed gels versus US-exposed gels at regions outside of the US beam width (Fig. 5B), demonstrating spatial specificity of the acoustic exposure. Cell adhesion to sham- (Fig. 5C) and US-exposed collagen gels (Fig. 5D) was inhibited by blocking antibodies directed against β$_1$, but not β$_3$ integrins. Adhesion to native type I collagen is mediated primarily through α$_{1/2}$β$_1$ integrins, whereas adhesion to thermally or enzymatically degraded collagen (i.e., gelatin) is mediated by α$_v$β$_3$ integrins [34]. Together, these results indicate that US exposure during collagen polymerization reduces initial cell attachment strength while maintaining β$_1$ integrin–binding specificity.

3.5. Acoustic modification supports cell-mediated remodeling of collagen gels

Cell migration on 3D substrates is a complex process involving bidirectional interactions between cells and the surrounding ECM [35]. Substrate cues such as collagen fiber alignment, pore size, and ligand-receptor interactions can direct cell migration, triggering cell-mediated remodeling of the surrounding matrix [11,32,36]. To investigate whether the increase in cell migration activity observed on US-exposed collagen gels was associated with cell-mediated remodeling of collagen fibers, we first asked whether the observed collagen fiber compaction was associated with multicellular aggregates. Panoramic images were assembled from overlapping images collected over an area corresponding to the 3-mm half-maximal beam width of the acoustic field. Cells seeded on collagen gels polymerized in the presence of US (7.8-MHz; 6.8 W/cm^2) migrated into radially aligned circular aggregates (Fig. 6A) that colocalized with collagen fiber bundles throughout the US-exposed region (Fig. 6B); cell-free areas were associated with reduced SHG intensity (Fig. 6B). Higher magnification images of cell-seeded, US-exposed gels showed cells distributed along the axis of collagen fiber bundles, with regions of increased SHG intensity surrounding cell clusters (Fig. 6C). In comparison, cells cultured on temperature-matched, sham-exposed gels remained evenly distributed and exhibited homogeneous SHG intensity, even at locations immediately adjacent to cells (Fig. 6D).

To further evaluate the ability of cells to remodel US-exposed collagen fibers, collagen hydrogels cultured in either the presence or absence of cells were labeled with CHPs. CHPs are synthetic molecules consisting of several collagen glycine-proline-hydroxyproline repeats tagged with a fluorescent probe [37] and have been used to assess collagen remodeling
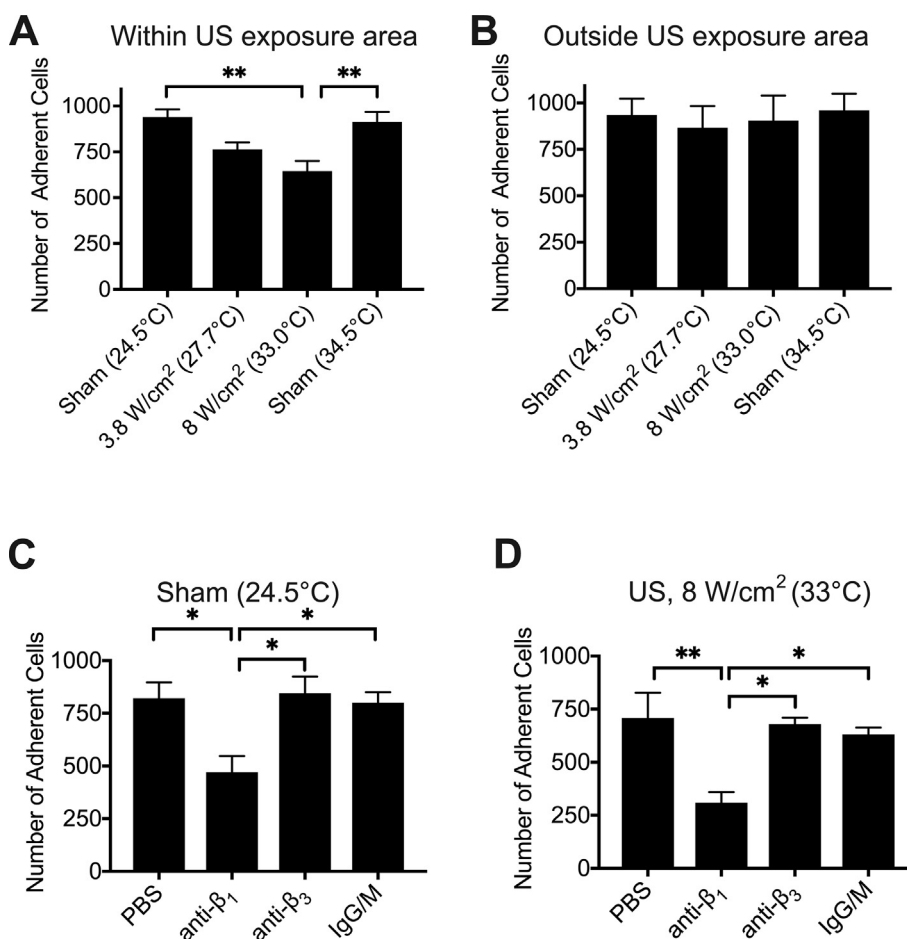

Fig. 5. Effects of ultrasound on substrate adhesive properties. Aliquots of collagen (2 mg/mL) were polymerized during exposure to 8.8-MHz ultrasound at intensities of 3.8 W/cm^2 or 8 W/cm^2 or were sham exposed with the water tank temperature set to produce temperature-matched controls. Maximum temperatures achieved are indicated in parentheses. FN-null MEFs (2 × 10^4 cells/cm^2) were seeded onto polymerized gels and allowed to adhere for 20 min. The number of adherent cells at locations corresponding to (A) the gel center or (B) a location outside of the ultrasound exposure area (5 mm off-center) was quantified. (C and D) FN-null MEFs were treated with anti-β$_1$ or anti-β$_3$ integrin antibodies, an equal volume of PBS, or the corresponding isotype controls, before seeding on collagen gels polymerized in the absence (sham) or presence of 8.8-MHz ultrasound (US) at an intensity of 8 W/cm^2. After 20 min, the number of adherent cells was determined. Data are presented as the mean ± SEM for n = 6 independent replicates per condition. Significantly different means, *P < 0.05 and **P < 0.01, by one-way ANOVA with the Bonferroni post hoc test. PBS, phosphate-buffered saline; FN-null MEFs, fibronectin-null mouse embryonic fibroblasts; ANOVA, analysis of variance; SEM, standard error of the mean; US, ultrasound.
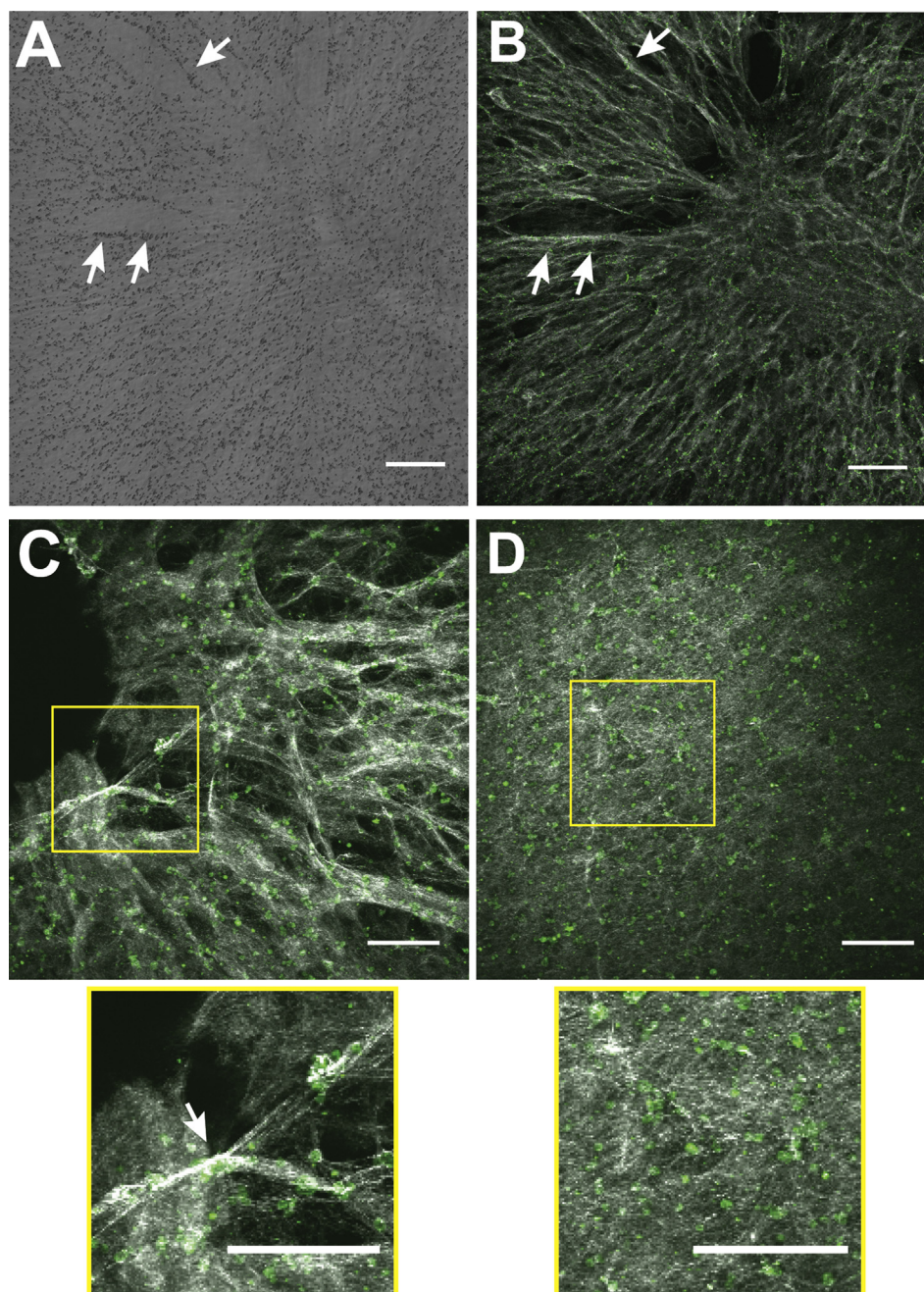
Fig. 6. Cell accumulation and collagen fiber compaction on ultrasound-exposed gels. Aliquots of soluble collagen were polymerized in the presence of 7.8-MHz ultrasound at an intensity of 6.8 W/cm^2 (A–C) or sham exposed in a 33 °C water tank (D). The peak temperature in both conditions was 30 °C. FN-null MEFs were seeded onto hydrogel surfaces and cultured for 24 h. Phase-contrast (A) and multiphoton (B–D) images were obtained. Maximum intensity projections were assembled from z-slices collected through a 100-μm depth (5-μm step size). (A and B) Overlapping images captured within the ultrasound-treated area of the same gel were merged to reconstruct an area representing the half-maximal ultrasound beam width (3 mm). (C and D) High-magnification images representing 1 of at least 3 samples fabricated on independent days. Insets (yellow) show detailed views, with arrows indicating area of cell-mediated collagen remodeling and cell aggregation. SHG, white; cells, green. Scale bars = 500 μm (A and B) or 200 μm (C and D). FN-null MEFs, fibronectin-null mouse embryonic fibroblasts; SHG, second harmonic generation.

in various tissues [38,39]. This sequence mimics the structure of a single collagen alpha chain and thus binds to native collagen after enzymatic degradation or upon unfolding of the triple helix via thermal or mechanical mechanisms [37,39]. In the absence of cells, limited CHP staining was detected on acellular collagen gels fabricated in the presence of US (Fig. 7A, -cells). However, addition of cells to US-exposed collagen gels resulted in CHP-positive fibers that corresponded to areas of increased SHG signal intensity (Fig. 7A, + cells), revealing areas of cell-mediated collagen fiber remodeling. In contrast, addition of cells to sham-exposed hydrogels had no effect on either SHG or CHP signals (Fig. 7B and S3), indicating that cells did not remodel the sham-exposed collagen. Together, these results provide evidence that US exposure alters the collagen microstructure in a manner that allows for cell-mediated remodeling. No differences in the overall intensity of CHP staining were observed between acellular, US-exposed gels and the corresponding temperature-matched, sham-exposed gels (Fig. 7A versus 7B, -cells)

These results indicate that US exposure during hydrogel fabrication does not directly alter the triple helical conformation of collagen, but rather sensitizes collagen to subsequent cellular remodeling.

3.6. Effect of acoustically modified collagen in a skin explant model of wound healing

Cell activities supported by acoustically modified collagen gels, including cell migration and collagen fiber remodeling, are critical for effective dermal wound healing [35,40]. To assess the biological activity of acoustically modified collagen in a system that incorporates a mixed population of cells from the primary wound environment, tissue explants derived from full-thickness skin punch biopsies of genetically diabetic mice were investigated. Tissue explants were placed on the surface of collagen hydrogels polymerized either in the presence of 7.8-MHz US at an intensity of 6.8 W/cm^2 or under temperature-matched, sham-exposure conditions
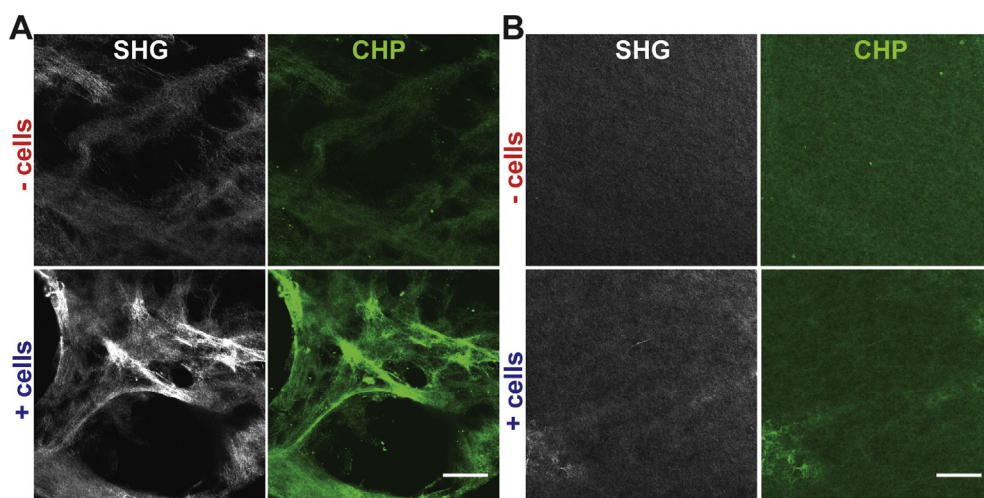
Fig. 7. Cell-mediated collagen fibril remodeling is enhanced in acoustically modified hydrogels. Collagen gels were polymerized during exposure to 8.8-MHz ultrasound (8 W/cm^2) in a 25 °C exposure chamber (A) or under sham conditions in a 37 °C exposure chamber (B). Gels were cultured for 24 h in media containing either no cells (-cells) or FN-null MEFs (4.7 × 10^4 cells/cm^2, + cells) before decellularization and staining with CHPs. Maximum intensity z-projections through a depth of 20 μm were assembled using FIJI software. Images represent 1 of at least 3 samples fabricated on independent days. Scale bars = 100 μm. SHG, second harmonic generation; CHP, collagen hybridizing peptide; FN-null MEFs, fibronectin-null mouse embryonic fibroblasts.

(Fig. 8A). The explants were cultured for 3 days, during which time, a mixed population of cells migrated out of the tissue and attached to the surfaces of both sham- and US-exposed gels (Fig. 8B). After 4 days, cells on sham-exposed gels remained adherent to the surface, with no apparent changes in the overall cell distribution or underlying gel surface (Fig. 8C, sham). In contrast, explant-derived cells cultured on collagen gels polymerized in the presence of US remodeled the underlying substrate to form dense, multicellular fibrillar bundles (Fig. 8C, US).
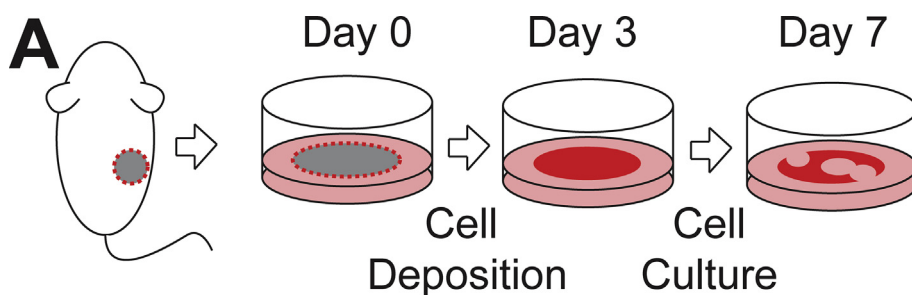

Fig. 8. Cell-mediated remodeling of acoustically modified collagen in a skin explant model of wound healing. (A) Full-thickness skin sections (6-mm diameter) were removed from the dorsal side of genetically diabetic mice and placed in contact with the surface of collagen hydrogels fabricated under sham or ultrasound (7.8 MHz, 6.8 W/cm^2) conditions. The final temperature achieved with both conditions was 30 °C. Explants were incubated for 3 days and then removed. Images of the gel surface were collected (B). Gels were reimaged on day 7 (C). Images represent 1 of at least 3 samples fabricated on independent experimental days. Scale bars = 100 μm. US, ultrasound.
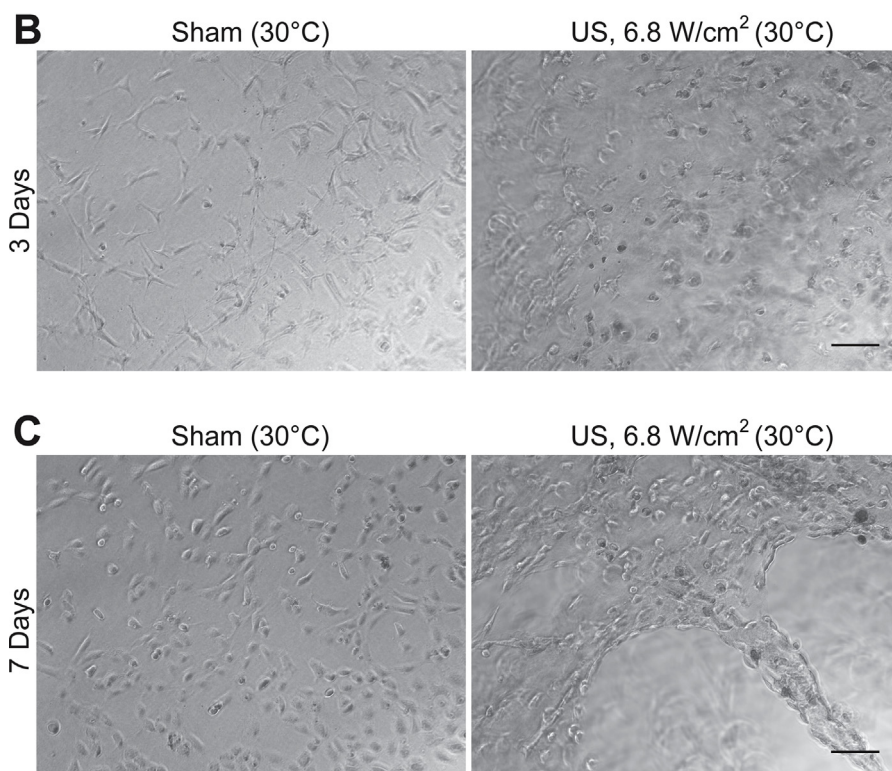
4. Discussion

In this study, we showed that polymerizing collagen hydrogels in the presence of US (7.8 or 8.8 MHz; 3.2–10 W/cm^2) produces local variations in collagen fiber structure and organization that support directed cell migration and cell-mediated collagen fiber remodeling. Cell migration and collagen fiber remodeling were not observed in sham-exposed, temperature-matched collagen gels, indicating that the observed effects of US arose from a mechanical rather than thermal mechanism. The strength of cell adhesion to US-exposed collagen was reduced compared with temperature-matched control gels. Importantly, at acoustic intensities used in the present study, US exposure did not denature fibrillar collagen as (i) cell adhesion to both US- and sham-exposed gels was mediated by β_1 integrins and (ii) in the absence of cells, similar levels of CHP staining was observed in US- versus sham-exposed gels. Rather, data indicate that US introduced subtle conformational changes to the triple-helical structure of collagen fibers that reduced the strength of cell-substrate attachments, which in turn facilitated cell migration and ECM remodeling [32]. Skin explants obtained from diabetic mice demonstrated similar enhancement of cell-mediated remodeling of US- but not sham-exposed collagen hydrogels. Thus, collagen hydrogels fabricated in situ using US may provide an improved scaffold for cell infiltration and native ECM remodeling for wound healing applications.

US fields can interact with biomaterials via heating, cavitation, and/ or mechanical forces [16]. In the present study, US exposure led to the formation of radially aligned collagen fibers that were not observed in temperature-matched control gels, suggesting an underlying mechanical mechanism (e.g., via acoustic streaming or cavitation) for effects of US on collagen bioactivity. Furthermore, the pattern of radial fiber alignment observed in these studies is consistent with experimental and simulation studies of US-induced fluid streaming patterns within cylindrical plastic containers [41], and in the present study, fluid streaming was evident during US exposures. Although the acoustic exposure geometry produced an US standing wave field within the exposure chamber, we found no evidence in our present or previous [21] study that effects of US on collagen were dependent on forces associated with a standing wave field. The results of the present study, together with previous investigations into the effects of US on collagen [21], indicate that non-thermal effects of US such as fluid streaming, as well as thermal effects of US, can function as two distinct mechanisms by which US influences collagen structure and organization. This has significant implications for the utility of acoustic techniques for manipulating the structure and function of collagen within engineered tissues as US parameters and exposure geometries might be optimized to favor either heating or fluid streaming within different regions of a 3D scaffold. As well, thermal and non-thermal effects of US may be combined synergistically to produce collagen-based hydrogels with greater complexity.

Tissue repair is a complex process requiring cells to migrate into the wound space while coordinating multiple and simultaneous tissue-remodeling behaviors, that include ECM deposition, contraction, and proteolysis [35,40]. The migration of cells on acoustically modified collagen hydrogels was associated with simultaneous changes in the underlying substrate, including collagen fiber contraction and conformational changes leading to enhanced CHP binding. These changes to the experimental substrate occurred under conditions designed to minimize collagen matrix deposition and therefore represent direct cellular remodeling rather than the assembly of new ECM components [31]. A number of reports have highlighted the importance of cell-derived tension as a central coordinator of wound healing behaviors within 3D ECM structures [42–44]. Of note, Sakar et al [42] recently described a micro-tissue model of wound healing that enabled monitoring of gap closure within suspended, fibroblast-embedded collagen gels. In these studies, generation of cell-derived tension within collagen matrices was a necessary prerequisite for gap repair via a fibronectin-mediated deposition process [42]. This finding raises the possibility that within a wound repair environment, tension-induced conformational changes in collagen may

serve as a template for subsequent fibronectin matrix deposition and tissue regeneration. The ability of acoustically modified collagen to potentiate ECM remodeling behaviors in both FN-null MEFs and skin explant–derived cells is a promising indicator that US may be used to generate engineered biomaterials that facilitate coordinated tissue repair.

5. Conclusion

Mechanical forces associated with US propagation enable localized manipulation of collagen fiber structure within 3D engineered biomaterials. This strategy can be used to produce functionally enhanced collagen hydrogels that support simultaneous cellular migration and ECM remodeling. Thus, US offers a promising non-invasive, rapid, and non-toxic technique for manufacturing improved therapeutic biomaterials, either alone or in combination with other methodologies.

Research data

Data will be made available upon request.

Declaration of interest

The authors declare that they have no known competing financial interests or personal relationships that could have appeared to influence the work reported in this paper.

Acknowledgments

Appendix A. Supplementary data

Supplementary data to this article can be found online at https://doi.org/10.1016/j.mtbio.2019.100018.

References

[1] K.E. Kadler, C. Baldock, J. Bella, R.P. Boot-Handford, Collagens at a glance, J. Cell Sci. 120 (2007) 1955–1958, https://doi.org/10.1242/jcs.03453.

[2] E.E. Antoine, P.P. Vlachos, M.N. Rylander, Review of collagen I hydrogels for bioengineered tissue microenvironments: characterization of mechanics, structure, and transport, Tissue Eng. Part B 20 (2014) 683–696. https://doi.org/10.1089/ten.teb.2014.0086.

[3] E.A. Abou Neel, L. Bozec, J.C. Knowles, O. Syed, V. Mudera, R. Day, et al., Collagen - emerging collagen based therapies hit the patient, Adv. Drug Deliv. Rev. 65 (2013) 429–456. https://doi.org/10.1016/j.addr.2012.08.010.

[4] L. Cen, W. Liu, L. Cui, W. Zhang, Y. Cao, Collagen tissue engineering: development of novel biomaterials and applications, Pediatr. Res. 63 (2008) 492–496. https://doi.org/10.1203/PDR.0b013e31816c5bc3.

[5] D.G. Wallace, J. Rosenblatt, Collagen gel systems for sustained delivery and tissue engineering, Adv. Drug Deliv. Rev. 55 (2003) 1631–1649. https://doi.org/10.1016/j.addr.2003.08.004.

[6] J. Glowacki, S. Mizuno, Collagen scaffolds for tissue engineering, Biopolymers 89 (2008) 338–344. https://doi.org/10.1002/bip.20871.

[7] S. Schleifenbaum, T. Prietzel, G. Aust, A. Boldt, S. Fritsch, I. Keil, et al., Acellularization-induced changes in tensile properties are organ specific - an in-vitro mechanical and structural analysis of porcine soft tissues, PLoS One 11 (2016), e0151223. https://doi.org/10.1371/journal.pone.0151223.

[8] K. Gelse, E. Poschl, T. Aigner, Collagens–structure, function, and biosynthesis, Adv. Drug Deliv. Rev. 55 (2003) 1531–1546. https://doi.org/10.1016/j.addr.2003.08.002.

[9] G.C. Wood, The formation of fibrils from collagen solutions. 2. A mechanism of collagen-fibril formation, Biochem. J. 75 (1960) 598–605.

[10] Y.L. Yang, S. Motte, L.J. Kaufman, Pore size variable type I collagen gels and their interaction with glioma cells, Biomaterials 31 (2010) 5678–5688. https://doi.org/10.1016/j.biomaterials.2010.03.039.

[11] S.P. Carey, C.M. Kraning-Rush, R.M. Williams, C.A. Reinhart-King, Biophysical control of invasive tumor cell behavior by extracellular matrix microarchitecture, Biomaterials 33 (2012) 4157–4165. https://doi.org/10.1016/j.biomaterials.2012.02.029.

[12] D.P. McDaniel, G.A. Shaw, J.T. Elliott, K. Bhadriraju, C. Meuse, K.H. Chung, et al., The stiffness of collagen fibrils influences vascular smooth muscle cell phenotype, Biophys. J. 92 (2007) 1759–1769. https://doi.org/10.1529/biophysj.106.089003.

[13] B.A. Roeder, K. Kokini, J.E. Sturgis, J.P. Robinson, S.L. Voytik-Harbin, Tensile mechanical properties of three-dimensional type I collagen extracellular matrices with varied microstructure, J. Biomech. Eng. 124 (2002) 214–222. https://doi.org/10.1115/1.1449904.

[14] B.C. Isenberg, R.T. Tranquillo, Long-term cyclic distention enhances the mechanical properties of collagen-based media-equivalents, Ann. Biomed. Eng. 31 (2003) 937–949.

[15] D. Miller, N. Smith, M. Bailey, G. Czarnota, K. Hynynen, I. Makin, et al., Overview of therapeutic ultrasound applications and safety considerations, J. Ultrasound Med. 31 (2012) 623–634. https://doi.org/10.7863/jum.2012.31.4.623.

[16] D. Dalecki, Mechanical bioeffects of ultrasound, Annu. Rev. Biomed. Eng. 6 (2004) 229–248. https://doi.org/10.1146/annurev.bioeng.6.040803.140126.

[17] National Council on Radiation Protection and Measurements, NCRP Report No. 140, Exposure Criteria for Medical Diagnostic Ultrasound: II. Criteria Based on All Known Mechanisms, 2002. Bethesda.

[18] H. Pauly, H.P. Schwan, Mechanism of absorption of ultrasound in liver tissue, J. Acoust. Soc. Am. 50 (1971) 692–699. https://doi.org/10.1121/1.1912685.

[19] S.A. Goss, F. Dunn, Ultrasonic propagation properties of collagen, Phys. Med. Biol. 25 (1980) 827–837. https://doi.org/10.1088/0031-9155/25/5/001.

[20] N. Saeidi, E.A. Sander, J.W. Ruberti, Dynamic shear-influenced collagen self-assembly, Biomaterials 30 (2009) 6581–6592. https://doi.org/10.1016/j.biomaterials.2009.07.070.

[21] K.A. Garvin, J. VanderBurgh, D.C. Hocking, D. Dalecki, Controlling collagen fiber microstructure in three-dimensional hydrogels using ultrasound, J. Acoust. Soc. Am. 134 (2013) 1491–1502. https://doi.org/10.1121/1.4812868.

[22] D. Dalecki, E.L. Carstensen, K.J. Parker, D.R. Bacon, Absorption of finite amplitude focused ultrasound, J. Acoust. Soc. Am. 89 (1991) 2435–2447. https://doi.org/10.1121/1.400976.

[23] T.G. Muir, E.L. Carstensen, Prediction of nonlinear acoustic effects at biomedical frequencies and intensities, Ultrasound Med. Biol. 6 (1980) 345–357. https://doi.org/10.1016/0301-5629(80)90004-6.

[24] F. Shi, J. Harman, K. Fujiwara, J. Sottile, Collagen I matrix turnover is regulated by fibronectin polymerization, Am. J. Physiol. Cell Physiol. 298 (2010) C1265–C1275. https://doi.org/10.1152/ajpcell.00341.2009.

[25] K.A. Garvin, D.C. Hocking, D. Dalecki, Controlling the spatial organization of cells and extracellular matrix proteins in engineered tissues using ultrasound standing wave fields, Ultrasound Med. Biol. 36 (2010) 1919–1932. https://doi.org/10.1016/j.ultrasmedbio.2010.08.007.

[26] M.A. Chernousov, M.L. Metsis, V.E. Koteliansky, Studies of extracellular fibronectin matrix formation with fluoresceinated fibronectin and fibronectin fragments, FEBS (Fed. Eur. Biochem. Soc.) Lett. 183 (1985) 365–369. https://doi.org/10.1016/0014-5793(85)80811-5.

[27] J.J. Leskinen, K. Hynynen, Study of factors affecting the magnitude and nature of ultrasound exposure with in vitro set-ups, Ultrasound Med. Biol. 38 (2012) 777–794. https://doi.org/10.1016/j.ultrasmedbio.2012.01.019.

[28] W.J. Fry, R.B. Fry, Determination of absolute sound levels and acoustic absorption coefficients by thermocouple probes—theory, J. Acoust. Soc. Am. 26 (1954) 294–310. https://doi.org/10.1121/1.1907332.

[29] K.A. Burke, R.P. Dawes, M.K. Cheema, A.V. Hove, D.S.W. Benoit, S.W. Perry, et al., Second-harmonic generation scattering directionality predicts tumor cell motility in

[30] collagen gels, J. Biomed. Opt. 20 (2015), 051024. https://doi.org/10.1117/1.JBO.20.5.051024.

[30] J. Sottile, D.C. Hocking, P.J. Swiatek, Fibronectin matrix assembly enhances adhesion-dependent cell growth, J. Cell Sci. 111 (1998) 2933–2943. https://doi.org/10.1083/JCB.133.2.391.

[31] J. Sottile, F. Shi, I. Rublyevska, H.Y. Chiang, J. Lust, J. Chandler, Fibronectin-dependent collagen I deposition modulates the cell response to fibronectin, Am. J. Physiol. Cell Physiol. 293 (2007) C1934–C1946. https://doi.org/10.1152/ajpcell.00130.2007.

[32] M.H. Zaman, L.M. Trapani, A.L. Sieminski, D. MacKellar, H. Gong, R.D. Kamm, et al., Migration of tumor cells in 3D matrices is governed by matrix stiffness along with cell-matrix adhesion and proteolysis, Proc. Natl. Acad. Sci. U.S.A. 103 (2006) 10889–10894. https://doi.org/10.1073/pnas.0604460103.

[33] J.R. Brennan, D.C. Hocking, Cooperative effects of fibronectin matrix assembly and initial cell-substrate adhesion strength in cellular self-assembly, Acta Biomater. 32 (2016) 198–209. https://doi.org/10.1016/j.actbio.2015.12.032.

[34] G.E. Davis, Affinity of integrins for damaged extracellular matrix: αvβ3 binds to denatured collagen type I through RGD sites, Biochem. Biophys. Res. Commun. 182 (1992) 1025–1031. https://doi.org/10.1016/0006-291X(92)91834-D.

[35] F. Grinnell, W.M. Petroll, Cell motility and mechanics in three-dimensional collagen matrices, Annu. Rev. Cell Dev. Biol. 26 (2010) 335–336. https://doi.org/10.1146/annurev.cellbio.042308.113318.

[36] P.P. Provenzano, D.R. Inman, K.W. Eliceiri, S.M. Trier, P.J. Keely, Contact guidance mediated three-dimensional cell migration is regulated by Rho/ROCK-dependent matrix reorganization, Biophys. J. 95 (2008) 5374–5384. https://doi.org/10.1529/biophysj.108.133116.

[37] Y. Li, C.A. Foss, D.D. Summerfield, J.J. Doyle, C.M. Torok, H.C. Dietz, et al., Targeting collagen strands by photo-triggered triple-helix hybridization, Proc. Natl. Acad. Sci. U.S.A. 109 (2012) 14767–14772. https://doi.org/10.1073/pnas.1209721109.

[38] J. Hwang, Y. Huang, T.J. Burwell, N.C. Peterson, J. Connor, S.J. Weiss, et al., In situ imaging of tissue remodeling with collagen hybridizing peptides, ACS Nano 11 (2017) 9825–9835. https://doi.org/10.1021/acsnano.7b03150.

[39] J.L. Zitnay, Y. Li, Z. Qin, B.H. San, B. Depalle, S.P. Reese, et al., Molecular level detection and localization of mechanical damage in collagen enabled by collagen hybridizing peptides, Nat. Commun. 8 (2017) 14913. https://doi.org/10.1038/ncomms14913.

[40] V. Falanga, Wound healing and its impairment in the diabetic foot, Lancet 366 (2005) 1736–1743. https://doi.org/10.1016/S0140-6736(05)67700-8.

[41] A. Green, J.S. Marshall, D. Ma, J. Wu, Acoustic streaming and thermal instability of flow generated by ultrasound in a cylindrical container, Phys. Fluids 28 (2016) 104105. https://doi.org/10.1063/1.4965899.

[42] M.S. Sakar, J. Eyckmans, R. Pieters, D. Eberli, B.J. Nelson, C.S. Chen, Cellular forces and matrix assembly coordinate fibrous tissue repair, Nat. Commun. 7 (2016) 11036. https://doi.org/10.1038/ncomms11036.

[43] A. Brugués, E. Anon, V. Conte, J.H. Veldhuis, M. Gupta, J. Colombelli, et al., Forces driving epithelial wound healing, Nat. Phys. 10 (2014) 683–690. https://doi.org/10.1038/NPHYS3040.

[44] S.R.K. Vedula, H. Hirata, M.H. Nai, A. Brugués, Y. Toyama, X. Trebat, et al., Epithelial bridges maintain tissue integrity during collective cell migration, Nat. Mater. 13 (2013) 87–96. https://doi.org/10.1038/nmat3814.